https://doi.org/10.20965/jrm.2020.p1279

Paper:

Tomato Growth State Map for the Automation of Monitoring and Harvesting

Takuya Fujinaga, Shinsuke Yasukawa, and Kazuo Ishii

Kyushu Institute of Technology
2-4 Hibikino, Wakamatsu, Kitakyushu, Fukuoka 808-0196, Japan
E-mail: fujinaga.takuya835@mail.kyutech.jp

[Received June 14, 2019; accepted October 12, 2020]

To realize smart agriculture, we engaged in its systematization, from monitoring to harvesting tomato fruits using robots. In this paper, we explain a method of generating a map of the tomato growth states to monitor the various stages of tomato fruits and decide a harvesting strategy for the robots. The tomato growth state map visualizes the relationship between the maturity stage, harvest time, and yield. We propose a generation method of the tomato growth state map, a recognition method of tomato fruits, and an estimation method of the growth states (maturity stages and harvest times). For tomato fruit recognition, we demonstrate that a simple machine learning method using a limited learning dataset and the optical properties of tomato fruits on infrared images exceeds more complex convolutional neural network, although the results depend on how the training dataset is created. For the estimation of the growth states, we conducted a survey of experienced farmers to quantify the maturity stages into six classifications and harvest times into three terms. The growth states were estimated based on the survey results. To verify the tomato growth state map, we conducted experiments in an actual tomato greenhouse and herein report the results.

Keywords: smart agriculture, agricultural robot, tomato growth state map, recognition, estimation

1. Introduction

In agriculture, a decrease in the number of farmers, an aging population, and a shortage of successors are significant problems. In response to such urgent problems, smart agriculture is expected to be an innovative method of utilizing robot technology and information communication technology. Some studies aiming to realize smart agriculture include the autonomous operation of agricultural machinery, automation of harvesting, and monitoring of the field environment and crops. For the autonomous operation of agricultural machinery, Noguchi proposed a robot farming system that utilizes intelligent robot vehicles to automate farming activities from planting to supplying products to consumers [1]. In addition to intelligent robot vehicles, they described the importance of simultaneous operations by developing a multiple robot system, safety when using robots, and management systems. For the automation of harvesting, Kondo et al. developed an end-effector that could harvest a tomato cluster [2]. In the results of harvesting experiments on a high-density plant training system, the harvesting time per cluster was 15 s, and the success rate of harvesting was 50% (10 tomato clusters out of 20). Yaguchi et al. developed an end-effector that grasped a fruit using grippers and plucked it from the separation layer in the peduncle [3]. They described the results of harvesting experiments conducted on an actual farm, demonstrating that the harvesting time was shortened by improving the harvesting motion. Yoshida et al. developed a robot that harvested a cluster of cherry tomatoes [4]. They focused on detecting the peduncles that the robot required when harvesting the clusters. The success rate of harvesting in experiments at an actual farm was 95% with seven clusters (19 tomato fruits out of 20 in seven tomato clusters). For the monitoring of the field environment and crops, Fukatsu et al. described a remote monitoring method that responded flexibly and dynamically to changes in the field environment for long-term field monitoring [5]. They established field servers, which are small monitoring sensor nodes, in some countries, and their effectiveness was reported. Fukui et al. developed a robot that estimated the volume of tomato fruits to create a database of fruit growth [6]. The robot detected fruits using saliency-based image processing and estimated the volume of the fruits. Furthermore, they designed multiple indicators to evaluate the precision of the estimation results. If the evaluation results are unreliable, the position for re-measurement is calculated. Studies aimed at realizing smart agriculture are diversifying, and various approaches using robot technology and information communication technology have been proposed.

Meanwhile, with the aging of agricultural workers, quantifying the expertise of experienced farmers is a significant concern. Choi et al. proposed a method of quantifying the maturity stages using image analysis [7]. They followed the classification standard of the maturity stages based on the color of the tomato fruit surface as defined by the United States Department of Agriculture (USDA). Comparing the results of the proposed method and manual grading, the rate correctly classified was 77.5% (93 tomato fruits out of 120). The USDA provides standards for both the maturity stages and size and quality tolerance as a guide to support farmers in improving the quality and marketability of their crops. Quantifying the maturity stages in these standards is synonymous with quantifying one of the farmers' main standards. Kusui et al. proposed the Agri-Info Science platform as a concrete system to address the necessity for skill transfer in response to various food problems associated with global population growth [8]. While many of the deep learning methods for harvest decisions focus only on images, experienced farmers have multiple criteria such as pruning and fruit thinning. The authors focused on assessments based on these criteria and developed an e-learning-based support system that enables inexperienced farmers to learn such advanced craftsmanship. Its effectiveness was demonstrated in an evaluation experiment of the learning support system for kiwi pruning operations. Wakamori et al. investigated the relationship between daily leaf wilting and stem diameter variation to estimate water stress on plants in water stress cultivation [9]. They also indicated that deep learning estimation methods are inadequate. Instead of adopting such black-box approaches, cross-correlation analysis was used to analyze the time lag correlation between leaf wilt quantified by optical flow and change in stem diameter as a water stress index. They demonstrated that the analysis results were consistent with known plant water transport mechanisms. Thus, to quantify the expertise of experienced farmers, conducting surveys of their insights and methods and experiments in an actual environment is important.

Our studies on the realization of smart agriculture were based on listening to the insights of experienced farmers in cooperation with the Hibikinada Green Farm Co., Ltd. (hereinafter, Hibikinada Green Farm), which implemented a long-term multi-stage cultivation of tomato plants by incorporating the cultivation technology developed in the Netherlands [10, 11]. We aimed to realize a system that uses robots to automate operations from the monitoring of tomato plants to harvest their fruits. **Fig. 1** shows an outline of this system. The robots move on a rail installed in a tomato greenhouse. The monitoring robot acquires the images of the cultivation area, and these data are sent to a database in cloud computing. The states of the tomato plants are estimated using these data. Subsequently, the harvesting robot harvests only the mature fruits. Thus, this system enables more efficient agriculture.

In this study, we aimed to generate a map of the tomato growth states that visualizes the relationship between the maturity stages, harvest times, and yield. Experienced farmers would designate the maturity stage of the tomato fruits to be harvested, and the yield would be predicted using this map. Furthermore, the harvesting robot can determine a harvesting strategy based on this map.

In this paper, to generate the tomato growth state map, we have described the generation method of the tomato

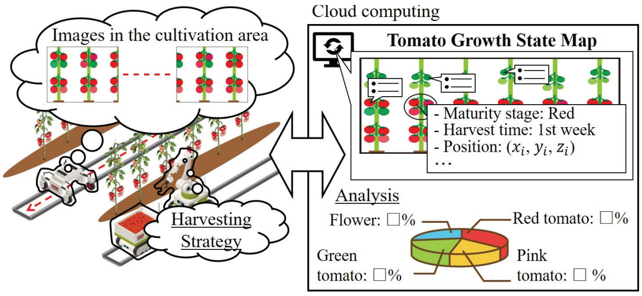

Fig. 1. Automation of monitoring the tomato plants and harvesting the tomato fruits.

growth state map, the recognition method of the tomato fruits, and the estimation method of the growth states (maturity stages and harvest times). The recognition rate (Accuracy) and detection rates (Precision, Recall, and F1-score) of the classifiers generated using different machine learning methods were compared. We focused on the characteristics of tomato fruits using infrared imaging to generate the classifiers. For the estimation method, we consulted experienced farmers of the Hibikinada Green Farm to decide the numbers of classifications for the maturity stages and terms for the harvest times. Subsequently, the growth states were estimated based on the results of the survey conducted to quantify their expertise. The proposed method is described in Section 2, the verification results of the tomato growth state map are detailed in Section 3. The findings are discussed in Section 4, and the conclusions are stated in Section 5.

2. Generation of the Tomato Growth State Map

2.1. Outline of the Generation Method

Figure 2 shows a flowchart for the generation of the tomato growth state map. The images (RGB, depth, and infrared) acquired by the robot were used as input (process (i), **Fig. 2**). First, pre-processing was conducted using depth imaging (process (ii), **Fig. 2**). Images focusing only on tomato plants in the target cultivation area were generated by removing the rear-row cultivation area and background on the RGB and infrared images. Next, a mosaic image composed of these images was generated (process (iii), **Fig. 2**). Tomato fruits on the mosaic image were detected (process (iv), **Fig. 2**), and the growth states (maturity stages and harvest times) of the detected fruits were estimated (process (v), **Fig. 2**). In addition, the position of the detected tomato fruits in the cultivation area was calculated using the coordinates in the mosaic image and depth data. Subsequently, the tomato growth state map was generated by adding the information of the tomato fruits to the mosaic image (process (vi), **Fig. 2**).

In Ref. [10], we proposed a method of generating a mosaic image, which is a single image generated by overlaying images with overlapping parts based on the results

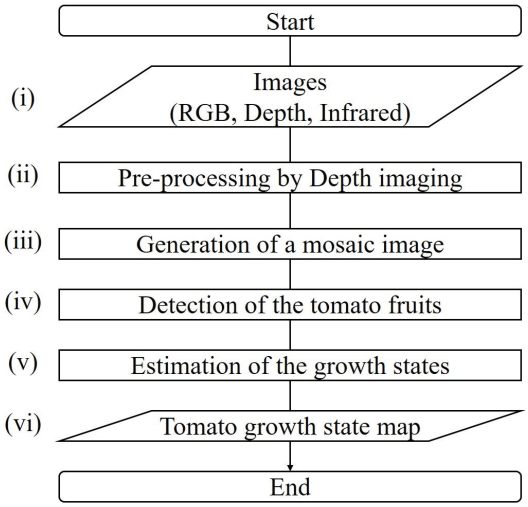

Fig. 2. Flowchart for the generation of the tomato growth state map.

of feature point matching. As a generation condition, the feature points extracted in the images must be distinguishable. However, objects (fruits, stems, leaves, etc.) in the tomato greenhouse are crowded together so that the matching rate is very low owing to similarities in the features. Therefore, generating a mosaic image with a simple matching method using RGB images is difficult. The proposed method improved the matching rate by limiting the depth direction using infrared imaging and limiting the search area of the feature points using the moving distance of the robot. Therefore, a mosaic image focusing on the target cultivation area was generated. In this paper, we present the steps to generate the tomato growth state map from processes (iv)–(vi) (**Fig. 2**).

This section describes the methods of recognizing tomato fruits and estimating their growth states. Previous studies on the recognition or detection of tomato fruits proposed methods focusing on the color, shape, and temperature of tomato fruits and methods using machine learning. Teimourlou et al. proposed a method of recognizing mature fruits using three color models (RGB, HIS, and YIQ) based on 200 RGB images acquired in a tomato greenhouse [12]. This method consists of two steps: removing the background of the image and extracting the mature fruits. The algorithm could extract 92%–96% of mature fruits. Hatou et al. proposed a method of recognizing mature and immature fruits using thermal imaging [13]. To recognize the fruits in the cluster individually, they applied a method based on wire size reduction and its effectiveness was demonstrated. Wang et al. proposed a method of recognizing mature fruits using a stereo vision system that employed the Otsu algorithm and elliptic template method [14]. The success rate of recognizing mature fruits was 99.3%, and the position of the fruits was calculated using feature point matching. Fujiura et al. proposed a method for recognizing mature and immature fruits using a dichromatic 3D vision sensor [15]. This sensor projected light of different wavelength bands and

Table 1. Comparison of previous studies.

First author	Detection (Rate [%])	Maturity stage	Harvest time	Fruit position
Teimourlou [12]	✓ (92–96)	1	–	–
Hatou [13]	✓ (–)	2	–	–
Wang [14]	✓ (99)	1	–	✓
Fujiura [15]	✓ (–)	2	–	✓
Yamamoto [16]	✓ (88)	2	–	–

the maturity stage was estimated using the difference in reflectance at each wavelength depending on the maturity stage. Yamamoto et al. proposed a method to detect young fruits as well as mature and immature fruits using machine learning-based methods (decision tree and X-means) [16]. The method achieved a Recall of 0.80 and Precision of 0.88.

To generate a map of the tomato growth states, we must detect the tomato fruits and estimate the maturity stages, harvest times, and position of the detected fruits. Based on these factors, **Table 1** shows a comparison of some functions in previous studies. The functions in **Table 1** are described as follows: the "Detection (Rate [%])" is whether or not the recognition or detection of tomato fruits are possible and their results based on the evaluation method of each study. The "Maturity stage" is how many stages the detected fruit is classified under; when it is one, only the mature fruits are classified and when it is two, the mature and immature fruits are classified. The "Harvest time" indicates whether or not the harvest time is estimated for the detected fruits. The "Fruit position" indicates whether or not the position of the detected fruit is calculated based on the world coordinate system. In **Table 1**, "✓" means that the function was achieved, and "–" means that it was not mentioned in the study. The method proposed in this paper achieved all these functions. This method recognizes tomato fruits regardless of the maturity stages using infrared imaging and estimates the maturity stages and harvest times using probability distributions quantified by combining the color value of the detected fruits with the expertise of experienced farmers.

2.2. Tomato Fruit Recognition

2.2.1. Optical Properties of Tomato Fruits on Infrared Images

We focused on the optical properties of tomato fruits as a method of recognizing them. Some studies recognized plant parts and evaluated maturity stages using the optical properties of plants. Kondo and Monta et al. measured the spectral reflectance properties of each part of the plants (fruit, leaves, stems, etc.) using a spectrophotometer capable of measuring light from the visible spectrum to a wavelength of 2500 nm [17, 18]. Experimental results demonstrated that specific wavelength bands are effective for recognizing specific plant parts. They also reported that, as tomato fruits mature, the reflectance from 500 to 600 nm decreases, and the reflectance around the chlorophyll absorption band at 670 nm increases. This indicates that the tomato fruit turns red as it matures. Li et al. classified tomato fruits into six maturity stages and reported the changes in the response of different reflection spectra to these various stages [19]. The responses change relatively significantly in the 400 to 700 nm range. Moreover, the responses in the six maturity stages are almost the same in the near-infrared range. Therefore, we focused on the optical properties of tomato fruits in the near-infrared range to recognize tomato fruits regardless of their maturity stages. Infrared images were acquired using a Microsoft Kinect sensor (hereinafter, Kinect), which is a time-of-flight camera that obtains images by projecting infrared light and measuring the time the projected light reaches an object and returns.

In addition, a known optical property of tomato fruits is that the central part has a strong response to the projected light and the peripheral parts have a weaker response. Ota et al. proposed a method of detecting tomato fruits by focusing on their optical properties [20]. This has been confirmed from experimental results of the reflection response of tomato fruits on the infrared image acquired using Kinect (Appendix A). Furthermore, experimental results have demonstrated that the infrared wavelength band of Kinect is effective in recognizing tomato fruits regardless of their maturity stage. In this proposed method, classifiers are generated by utilizing the optical properties of tomato fruits on infrared images.

2.2.2. Classifiers Utilizing the Optical Properties of Tomato Fruits

Three methods were verified as classifiers generated by utilizing the optical properties of tomato fruits on infrared images. In the first (hereinafter, classifier 1), histograms of oriented gradients (HOG) features were extracted from the input image and the features were classified using a support vector machine (SVM), which is a pattern recognition model [21, 22]. The second (classifier 2) was generated by learning a five-layer convolutional neural network (CNN) constructed by referring to the network architecture of LeNet, which is the basis of the CNN [23]. The third (classifier 3) was generated by transfer learning for GoogLeNet, which is a 22-layer CNN that was pre-trained using the ImageNet dataset [24, a]. We used MATLAB to implement these classifiers.

Here, the dataset is described. Images of tomato fruits or other objects (stems, leaves, etc.) were extracted from 50 infrared images acquired by a robot in the Hibikinada Green Farm. **Fig. 3** shows an example of images of positive and negative data. For the positive data in **Fig. 3(a)**, the images were extracted based

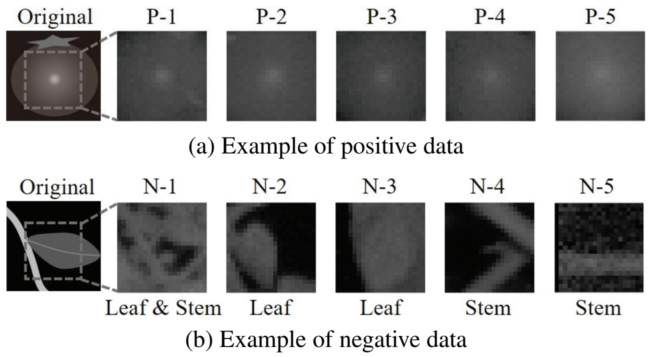

Fig. 3. Example of the dataset.

Table 2. Breakdown of the dataset.

	Positive data	Negative data
Training data	479	1536
Test data	205	658
Total	684	2194

on the center point of the fruits with the largest reflection response to the infrared light. For the negative data in **Fig. 3(b)**, the images were extracted from parts other than the tomato fruits on the infrared image. The resolution of the dataset was 21×21 pixel. It was defined as the resolution at which the optical properties of the tomato fruits on the infrared image (512×424 pixel) can be sufficiently confirmed. A breakdown of the dataset is summarized in **Table 2**. The numbers of positive and negative data were 684 and 2194, respectively. Among them, for the training data, 479 were positive data and 1536 were negative data, and for the test data, 205 were positive data and 658 were negative data.

Classifier 1 was generated using the linear SVM with the HOG features as the input. The output value in the linear SVM was 1 (tomato fruits) or 0 (not a tomato fruit). The HOG features were extracted by calculating the gradient direction and intensity of the brightness of the input image, creating histograms of the gradient for each cell, and normalizing by block. The input image was divided into blocks, and each block was composed of cells. The dimension of the HOG features (D_{HOG}) was calculated using the following equation:

$$D_{HOG} = {N_{BPI}}^2 {N_{block}}^2 N_{bin}, \quad \quad (1)$$

where N_{BPI} is the number of blocks per image, N_{block} is the number of cells in a block width, and N_{bin} is the number of gradient directions. N_{BPI} is calculated using the following equation:

$$N_{BPI} = \frac{\frac{N_{width}}{N_{cell}} - N_{block}}{N_{block} - N_{BO}} + 1, \quad \quad (2)$$

where N_{width} is the number of pixels in the width of the input image, N_{cell} is the number of pixels in a cell width, and N_{BO} is the number of cells overlapping adjacent blocks,

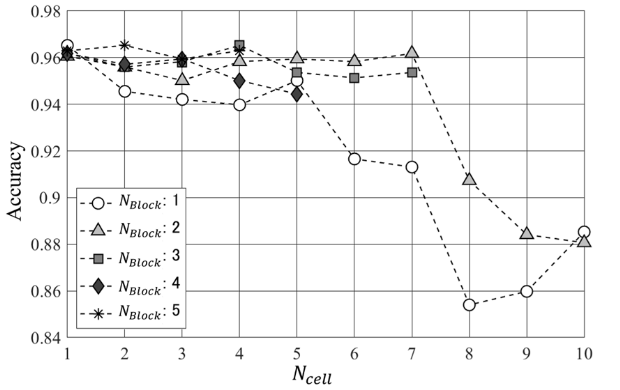

Fig. 4. Comparison of accuracy by varying the N_{cell} and N_{block}.

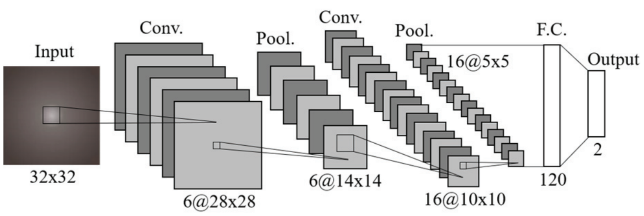

Fig. 5. Architecture of referencing the LeNet.

which is calculated using the following equation:

$$N_{BO} = \frac{N_{block}}{2}. \quad \ldots \ldots \ldots \ldots \quad (3)$$

N_{BPI} is rounded toward negative infinity and a valid value only for a positive value. N_{BO} is rounded toward negative infinity when N_{block} is one, and rounded toward positive infinity when N_{block} is one or more. In the extraction of HOG features, although the ratio of width and height in the size of the input image, block, and cell is basically arbitrary, we defined that the ratio is the same in this study. We fixed N_{width} and N_{bin} at 21 and nine, respectively, and focused on N_{cell} and N_{block}. To optimize these parameters, we evaluated the recognition rate by varying them. The results are shown in **Fig. 4**. The accuracy represents the correct rate of the classification results for the categories (positive or negative) labeled on the test data. If the HOG features cannot be extracted using Eq. (1) (e.g., N_{block} is four and N_{cell} is six), no data exists. The highest accuracy is 0.965 when N_{block} is three and the N_{cell} is four, and N_{block} is five and the N_{cell} is two. Here, focusing on D_{HOG} in these scenarios, the former is 729 and the latter is 2025 from Eq. (1). Moreover, the results are stable when N_{cell} is one regardless of N_{block}. Because N_{cell} is one pixel, the histograms are calculated for each pixel, and they are normalized by N_{block}. Therefore, more characteristics of tomato fruits on the infrared image can be extracted, and the recognition rate result is stable. However because the histogram is created for each pixel, D_{HOG} becomes large. Because the processing is faster when D_{HOG} is lower, we extract the HOG features with a N_{block} of three and N_{cell} of four.

For classifier 2, **Fig. 5** shows the architecture of referencing the LeNet with the 5-layer CNN. The convolutional layer (Conv.) and pooling layer (Pool.) are repeated twice, and finally, through the fully connected layer (F.C.), the probability of being classified as tomato fruits and other objects is the output. Although the sigmoid function is used as an activation function in LeNet, the ReLU function was used in this study. In addition, although LeNet reduces the data size of each layer by subsampling, max pooling was adopted in this study. For the resolution of the images (32×32, 28×28, 14×14, 10×10, and 5×5 pixel in **Fig. 5**), the number of feature maps in this architecture (6 and 16 in **Fig. 5**), and the dimension of the fully connected layer (120 in **Fig. 5**), the values of LeNet were referenced. Although the dataset is 21×21 pixel in **Table 2**, it was resized to 32×32 pixel to follow the architecture of LeNet. The output was a value in the range of 0.0 to 1.0, using the softmax function, which was classified as tomato fruits and other objects. The result depended on the setting of the threshold value for the output. In this study, the threshold value was set at 0.99. The network was trained using stochastic gradient descent with momentum with an initial learning rate of 0.0001. The maximum number of epochs was set to 30.

For classifier 3, GoogLeNet, which is a 22-layer CNN, was trained using ImageNet containing more than 14 million images for general object recognition and was retrained using the training dataset shown in **Table 2** for tomato fruit recognition. The input image was resized from 21×21 to 224×224 pixel, adjusted to be the same as GoogLeNet. The output had a value in the range of 0.0 to 1.0 as with classifier 2. The threshold value in classifier 3 was set to 0.99. The network learning method was the same as for classifier 2.

Here, for the threshold value, if the threshold value was changed, the results were changed. In this study, the threshold value was determined by prioritizing the result of the F1-score in the detection method described in Section 2.2.3.

2.2.3. Evaluation of the Classifiers

Two approaches were used to evaluate the three classifiers: the recognition rate (focusing only on Accuracy) when using the test data in **Table 2**, and the detection rates (focusing on the Precision, Recall, and F1-score) when detecting tomato fruits using the images acquired at the Hibikinada Green Farm. The recognition rate was the correct rate of the classification results for the categories (positive or negative) labeled on the test data. The detection method for the detection rates is shown in **Fig. 6**. The infrared image (521×424 pixel) was the input (process (i), **Fig. 6**), and the sliding window method was adopted to detect tomato fruits in the input image (process (ii), **Fig. 6**). With this method, a small region was scanned on the input image for each fixed pixel, and a classification result (tomato fruits or other objects) was output for each small region. Here, the number of fixed pixels when scanning a small region was called a step. The detection rates depended on the number of steps. In this study, we set the number to 1 pixel (here, called the

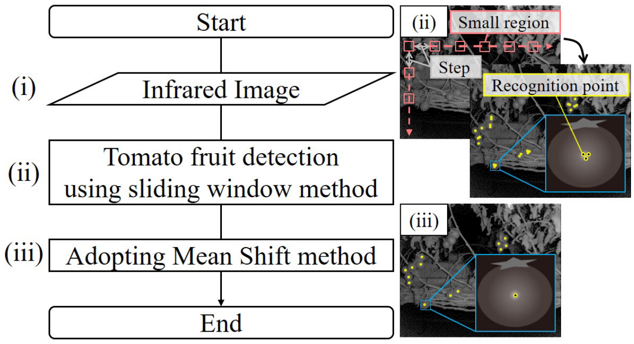

Fig. 6. Flowchart of tomato fruit detection.

entire search) to evaluate the classifiers, although the computation times were large. The resolution of the small region was 21×21 pixel, which was the same as the dataset. As shown in process (ii) of **Fig. 6**, one fruit may have two or more recognition points. Therefore, we adopted the mean shift method, which is an efficient and robust solution to the mode search problem, to converge two or more recognition points into one recognition point (process (iii), **Fig. 6**) [25].

Table 3 shows the input dimensions of each classifier and the results of the recognition and detection rates. Accuracy was the result when the test data in **Table 2** was used, and Precision, Recall, and F1-score were the results when 30 infrared images were used (test data and the 30 infrared images were different). The most accurate as well as the highest F1-score, which had a trade-off relationship with Precision and Recall, was classifier 1. In this study, 50 infrared images were used to create the dataset, although neural network with deep layers require more training data [a]. Therefore, when the entire search was performed, the unlearned data was the input, and the detection rates became lower than the recognition rate. Moreover, these results indicated that high recognition and detection rates in classifier 1 could be obtained even with a limited dataset and simple pattern recognition model by focusing on the optical properties of the tomato fruits and extracting the characteristics in advance. In this study, classifier 1 was used as a method for recognizing the fruits by considering the recognition rate, detection rates, and input dimension.

2.3. Growth State Estimation

2.3.1. Survey of Experienced Farmers

The growth states (maturity stages and harvest times) were added to the mosaic image based on the results of the surveys of experienced farmers at the Hibikinada Green Farm. These farmers can predict the yield in the tomato greenhouses based on the tomato growth state map by designating the maturity stages of the tomato fruits to be harvested. Moreover, they can create a shipping plan based on the demand forecasts from their clients and adjust production to reduce food loss by obtaining the harvest times for the fruits from this map.

Table 3. Comparison of the results in each classifier.

Classifier (Dim.)	Recognition rate	Detection rate		
	Accuracy	Precision	Recall	F1-score
1 (769)	0.965	0.934	0.775	0.847
2 (1,024)	0.931	0.711	0.769	0.739
3 (50,176)	0.957	0.651	0.610	0.630

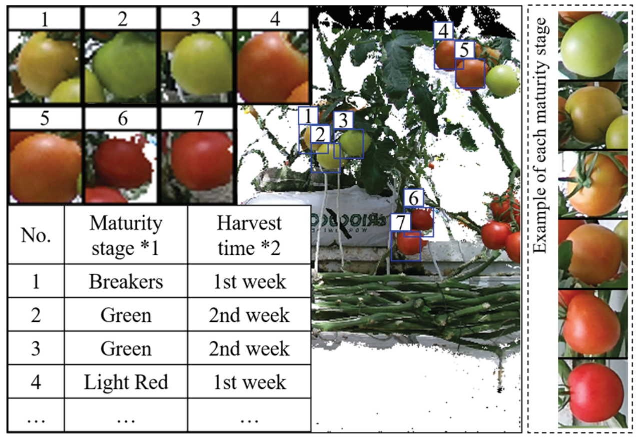

*1 Maturity stage: Green, Breakers, Turning, Pink, Light Red, Red
*2 Harvest time: 1st week, 2nd week, 3rd week, 4th week

Fig. 7. Examples of images used in the survey.

The numbers of classifications for the maturity stages and terms for the harvest times were determined by discussions with experienced farmers. The USDA has categorized the maturity stages into six classifications based on the color of the fruit surface: "Green," "Breakers," "Turning," "Pink," "Light Red," and "Red." Choi et al. used these as an index to assess the maturity stages, and Li et al. used them to investigate the response of the reflectance spectra [7, 19]. We also focused on these six maturity stages. Next, the harvest times are described. The tomato growth state map in this study focused on the area (80–120 cm from the ground in height) where the workers can easily harvest the fruits. The harvest times within this area are known to the farmers from the 1st to the 2nd weeks. However, fruits are still harvested even after these two terms; therefore, the harvest times are divided into four terms: the 1st, 2nd, 3rd, and 4th weeks.

We conducted the survey with the cooperation of nine experienced farmers at the Hibikinada Green Farm to quantify the growth states based on their expertise.

In this survey method, the experienced farmers were asked to select the maturity stages and harvest times that they considered suitable for the fruits in the images (**Fig. 7**). For example, for fruit number one in **Fig. 7**, the experienced farmer selected Breakers for maturity stage and 1st week as harvest time. In this survey, we asked nine experienced farmers for their insights and used 50 images existing 684 fruits in total (each image was structured as shown in **Fig. 7**).

Image and Hue of each tomato fruit						
No.	1	2	3	4	5	6
Image						
Hue	0.00	0.025	0.050	0.10	0.20	0.30
Answer results						
A	Red	Light Red	Pink	Turning	Breakers	Green
B	Red	Light Red	Pink	Breakers	Breakers	Green
C	Red	Pink	Turning	Turning	Green	Green

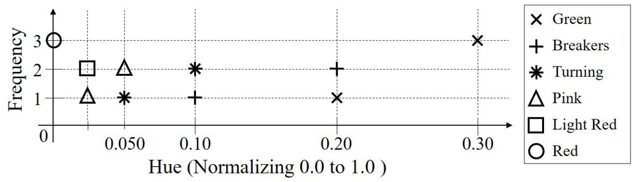

Fig. 8. Example of survey results.

2.3.2. Survey Results and Their Quantification

The color value of the tomato fruits on the images used in the survey was linked to the survey results of experienced farmers. **Fig. 8** is an example showing the survey results for the maturity stages of respondents A, B, and C for each tomato fruit. The results are summarized by defining the color value on the horizontal axis and the frequency of the number of respondents on the vertical axis. Here, the hue on the horizontal axis is normalized from 0.0 to 1.0. For example, for fruit number one in **Fig. 8**, all respondents selected Red, so the frequency of Red was three for hue 0.00.

The survey results for the maturity stages and harvest times are shown in **Figs. 9(a)** and **10(a)**, respectively. There were apparent false answers in this survey, e.g., Green as selected for mature fruits. Therefore, to quantify the expertise of experienced farmers using these results, we had to extract only the valid data. In this study, the frequency of the number of respondents as valid data was defined as one-third or more of the total number of respondents, i.e., three or more. In this definition, for the harvest times, since the frequency of selecting the 4th week was low, it was redivided into three terms: 1st, 2nd, and 3rd weeks.

The probability distribution of each valid data at each maturity stage and harvest time was calculated based on the probability density function $f(x)$, as follows:

$$f(x) = \frac{1}{\sqrt{2\pi\sigma^2}} \exp\left(-\frac{(x-\mu)^2}{2\sigma^2}\right), \quad . \ . \ . \ . \quad (4)$$

where x is the color value (hue), μ is the average of valid data at each maturity stage or harvest time, and σ is their standard deviation. The analysis results of the maturity stages and harvest times are shown in **Figs. 9(b)** and **10(b)**, respectively. The maturity stages and harvest times for the detected fruits were estimated by the ranges using points intersections of the adjacent probability density functions for each maturity stage and harvest time.

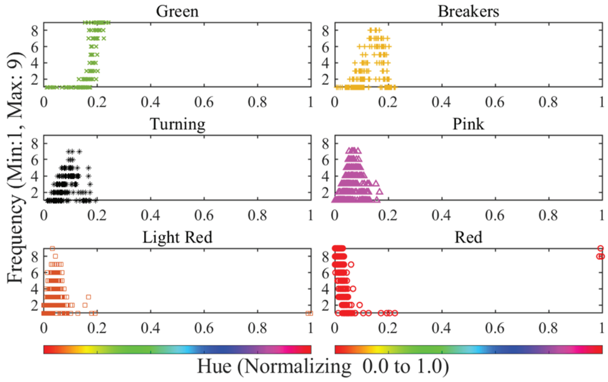

(a) Results of maturity stages in this survey

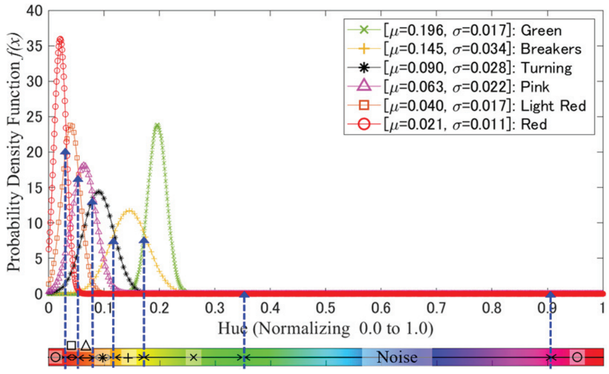

(b) Probability distribution at each maturity stage

Fig. 9. Results of the maturity stages.

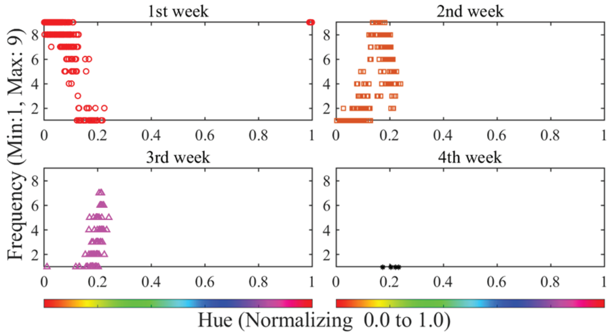

(a) Results of harvest times in this survey

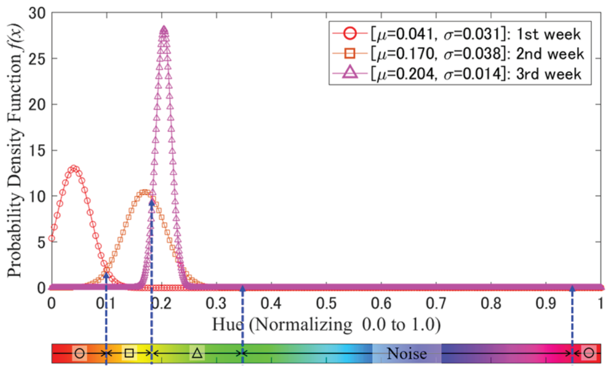

(b) Probability distribution at each harvest time

Fig. 10. Results of the harvest times.

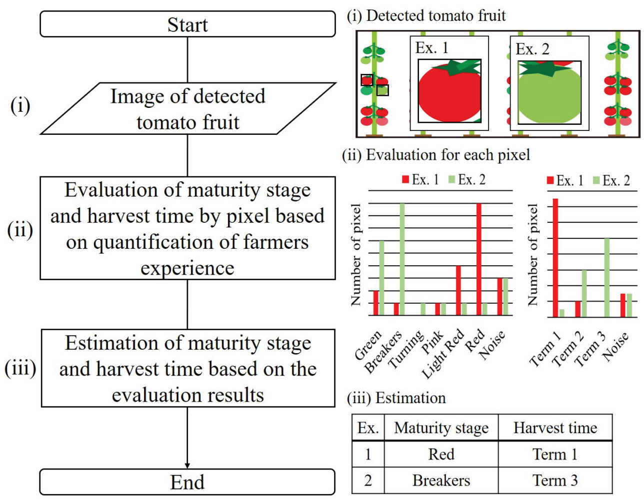

Fig. 11. Estimation method of maturity stages and harvest times.

That is, the hue of each pixel in the detected fruit image was inputted into the probability density function of each maturity stage and each harvest time, and those with the highest values are determined to be the maturity stage and harvest time for the pixel. However, for Red and Green in the maturity stages and the 1st and 3rd weeks in the harvest times, to decide the thresholds in both ends, we used 10σ (the quantification limit) of each probability density function. Here, since the hue was normalized from 0.0 to 1.0, the left end of Red and the 1st week were negative, and one was added to these values.

2.3.3. Estimation Method

Figure 11 shows a method to estimate the maturity stages and harvest times: "Term 1," "Term 2," and "Term 3" represent the 1st, 2nd, and 3rd weeks, respectively. The region in which the fruits were detected was used as an input image (process (i), **Fig. 11**), and the image was analyzed for each pixel based on the probability distribution described in Section 2.3.2 (process (ii), **Fig. 11**). The resolution of the input image was 10×10 pixel based on the center coordinates of the detected fruits. This was because 10×10 pixel was half the resolution of the fruit area (21×21 pixel) on the image, considering that the target fruits overlapped with other fruits in the clusters. The hue of each pixel was inputted to the probability density function of each maturity stage and each harvest time, and the maturity stage and harvest time at which the value was the highest were the classification results of the pixel. When the hue as an input fell outside the threshold of the maturity stage and harvest time, i.e., if it exceeded the quantification limit, that pixel was considered to be noise. The results analyzed for each pixel were constructed into a histogram, and the one with the highest frequency was used as the maturity stage and harvest time of the fruit (process (iii), **Fig. 11**). In the histogram of the fruits in Ex. 1 of **Fig. 11**, the results indicated that the distribution was high for Red as the maturity stage and Term 1 as the harvest time.

3. Evaluation of the Tomato Growth State Map

To evaluate the effectiveness of the tomato growth state map, we conducted experiments at the Hibikinada Green Farm from July 6 to August 4, 2020, targeting 30 tomato plants. The map was generated before harvesting work on July 6, 2020, and the results are reported in this paper for that date. A part of the tomato growth state map generated on July 6, 2020 is shown in **Fig. 12**. This map was the result of tomato fruit detection and growth state estimation performed on a mosaic image composed of 50 images. The illuminance was measured every time the image was acquired, and the average illuminance in the experiments was 0.9k lx and the standard deviation was 0.4k lx. In **Fig. 12**, the growth states ("M.S." and "H.T." mean the maturity stage and harvest time, respectively) and the position ("Pos." indicates the x, y, and z coordinates in the world coordinate system; the unit is meter) are clearly shown for three representative fruits among the detected fruits, but all the detected fruits have the same information.

Table 4 shows the detection rates (Precision, Recall, F1-score) and the estimation results for the maturity stages and harvest times. In this map, 136 tomato fruits were confirmed and 104 could be detected. The number of false recognition points was 11. For the detection rate results, the F1-score was 0.829. The maturity stages and harvest times of the detected fruits (104 fruits) were estimated. **Table 5** shows a comparison of the estimation results and actual number of harvested fruits. "Estimation" is the estimation results for the proposed method and "Actual" is the actual results. Additionally, the term 4th week is deemed invalid, as described in Section 2.3.2. However, since there was one scenario in the actual results, this term was added to **Table 5**. For the "Yield," we compared the number of actual harvested fruits and the estimation results based on the maturity stages Pink as designated by experienced farmers on July 6, 2020. The Yield of the Estimation (53, **Table 5**) was the total number of Pink (14, **Table 4**), Light Red (24, **Table 4**), and Red (15, **Table 4**) tomato fruits in the tomato growth state map. For the harvest times, we compared the estimation results and actual harvest times based on the date when the tomato growth state map was generated (July 6, 2020) by recording the growth states of the detected fruits after this date.

4. Discussion

4.1. Comparison with Previous Studies

Table 6 shows the results of this method for the functions mentioned in Section 2.1. "Detection (Rate [%])" refers to the F1-score in **Table 4**. For the six classifications in the "Maturity stage," they represent Green, Breakers, Turning, Pink, Light Red, and Red as defined by the USDA. To generate the tomato growth state map, this proposed method achieved all the functions. In particular, this study contributed to achieving the estimation of har-

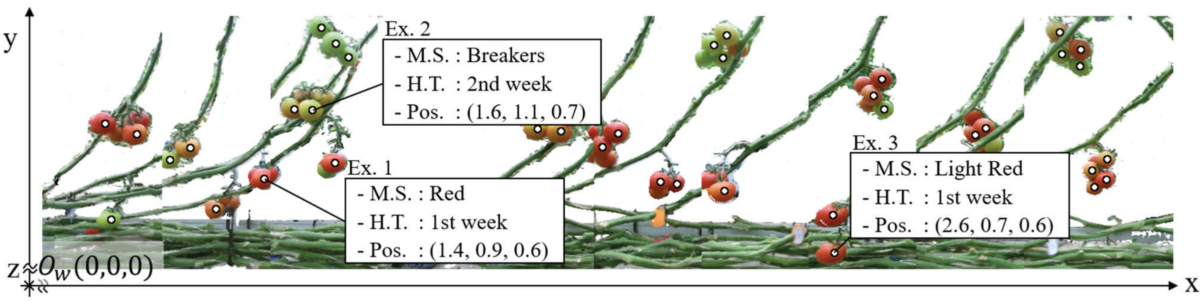

Fig. 12. Tomato growth state map.

Table 4. Results in the tomato growth state map.

Detection rates	
Precision	0.904 $\left(\frac{104}{115}\right)$
Recall	0.765 $\left(\frac{104}{136}\right)$
F1-score	0.829
Maturity stages	
Green	32
Breakers	5
Turning	14
Pink	14
Light Red	24
Red	15
Harvest times	
1st week	66
2nd week	20
3rd week	18

Table 5. Comparison of estimation results and the actual number of harvested fruits.

	Estimation	Actual
Yield	53	48
1st week	66	65
2nd week	20	38
3rd week	18	0
4th week	–	1

vest time, which could not be achieved by previous studies (**Table 1**).

4.2. Comparison of Detection Results and Actual Harvest

In the experiments, 30 tomato plants were targeted, and 205 tomato fruits were confirmed among the tomato plants. However, 136 tomato fruits were confirmed in the tomato growth state map. This was because of the mosaic image generation method. Frequently, a mosaic image was generated using images captured at a location at which the distance from the camera to the object is sufficiently large. In contrast, in the tomato greenhouse, the distance from the camera to the tomato plants (tomato fruits, leaves, stems, etc.) was relatively close, and this distance was not constant. Therefore, when the images were overlaid, they had discontinuities between them [10]. In addition, since the mosaic image used a single-viewpoint image, some fruits could not be confirmed in the image owing to occlusion between fruits in the tomato clusters or owing to leaves or stems. However, the mosaic image was generated using images captured at adjacent points and with overlapping regions, i.e., multi-viewpoint images were acquired for certain tomato fruits or clusters. **Fig. 13** shows the scenario in which images were acquired at positions P_1 and P_2. **Figs. 13(i)** and **(ii)** indicate the viewpoints of the cultivation area in the tomato greenhouse from the front and top views, respectively. For position P_1, fruits number one to three of the center tomato cluster in **Fig. 13(iii)** were confirmed.

Table 6. Evaluation of the proposed method.

	Detection (Rate [%])	Maturity stages	Harvest times	Fruit position
Proposed method	✓ (83)	6	✓	✓

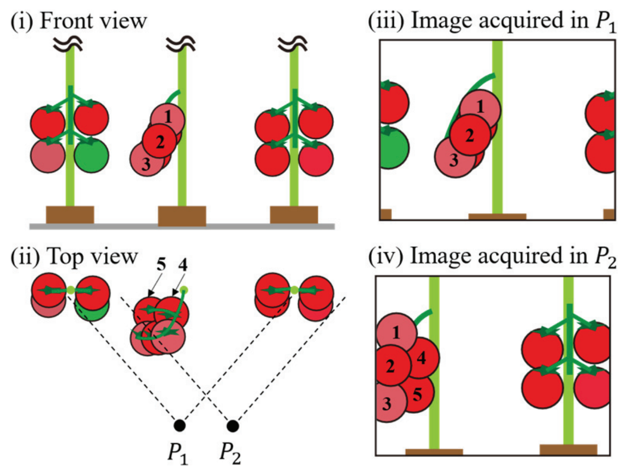

Fig. 13. Existence of the occlusion of tomato fruits depending on the image acquisition position.

In contrast, for position P_2, all the tomato fruits, i.e., fruits numbers one to five of the center tomato cluster in **Fig. 13(iv)**, were confirmed.

Therefore, we examined the actual tomato fruits and detected tomato fruits in each of the 50 images used to generate the mosaic image for this study. Each fruit in these images was identified and counted: 198 fruits were identified out of an actual count of 205, while 165 fruits out of the 198 were detected with the proposed method. Seven fruits could not be completely confirmed owing to occlusion. We can conclude that when generating the mosaic image, each fruit can be identified based on the position information of the fruits, and information on the hidden fruits is then added to the map.

4.3. Estimation Results

The total number of fruits at the Pink maturity stage or higher designated by the experienced farmers was 53, whereas the actual fruits harvested were 48. The workers harvest each tomato fruit in approximately 4 s, but the time to judge its maturity stage is only a moment. Therefore, in some scenarios, the tomato fruits to be harvested are missed, or a decision to not harvest it is made. The actual number of harvests without variation can be estimated using this estimation method based on the expertise of experienced farmers.

For harvest time, 66 fruits were estimated to be the 1st week whereas 65 fruits were actually harvested so that the estimated results were equivalent to the actual results. In contrast, for the 2nd and 3rd weeks in **Table 5**, the estimated result was 20 fruits for the 2nd week and 18 fruits in the 3rd week, but in the actual harvest, there were 38 fruits for the 2nd week. In the survey to quantify the expertise of experienced farmers, we asked them to make decisions based on the images; however, they also cultivated tomato plants in consideration of daily changes in temperature, humidity, and other factors. Therefore, we observed that they had difficulty making an estimation only by judging the images.

In addition, one fruit was harvested in the 4th week and it required four weeks to attain maturity. Thus some tomato fruits grow irregularly. On the other hand, almost all of the tomato fruits from 80 to 120 cm from the ground were harvested within two weeks based on the date when the tomato growth map was generated. The position of the tomato fruits on the map and harvest times may be closely related. In the future, we will propose an estimation method that considers images and environmental factors such as temperature and humidity, as well as focus on the position of tomato fruits, to clarify the relationship between fruit position and harvest time.

5. Conclusion

In this study, we aimed to realize a system that uses robots to automate farming processes by monitoring the growth states to harvest tomato fruits. The generation method for a map of the tomato growth states, used for the growth management of tomato plants and decision of harvesting strategies for robots, is described in this paper. The tomato growth state map was evaluated through experiments in an actual tomato greenhouse, and we demonstrated its effectiveness.

For tomato fruit recognition, we demonstrated that a simple machine learning method with a limited learning dataset exceeded the recognition results of the more complicated CNN using the optical properties of tomato fruits on infrared images. Although the sliding window method was applied to evaluate these classifiers, the method is inferior to other deep learning detection methods in terms of computation times [26, 27]. To implement the proposed method in the system, we must consider the computation times.

For growth state estimation, the maturity stages and harvest times were quantified based on a survey of experienced farmers. The proposed method proved to be effective for short-term estimations (the number of harvests on a certain day and the harvest time of the 1st week). In addition, we observed that even experienced farmers have difficulties estimating the long-term state of the fruits and harvest times for the 2nd week or 3rd week when using only image information. Further studies are underway to analyze both the images and environmental factors (temperature, humidity, etc.) and position of the tomato fruits to evaluate fruit growth states for both short- and long-term estimations. In addition, in the estimation method, the highest frequency of growth state was used as the output result from the histogram of each pixel in the input image, but this method could not utilize the distribution of the histogram. A future task we must consider is an estimation method using the distribution of each pixel on the input image.

Acknowledgements

In this survey and the experiments, we received cooperation from the Hibikinada Green Farm Co., Ltd., Hideyuki Ikari, Kazushi Kawajiri, and Keisuke Kimoto. We would like to express our sincere gratitude for their kind assistance. This work was supported by a Grant-in-Aid for JSPS Fellows 19J10900.

References:

[1] N. Noguchi, "Agricultural Vehicle Robot," J. Robot. Mechatron., Vol.30, No.2, pp. 165-172, 2018.

[2] N. Kondo, K. Yata, M. Iida, T. Shiigi, M. Monta, M. Kurita, and H. Omori, "Development of an End-effector for a Tomato Cluster Harvesting Robot," Engineering in Agriculture, Environment and Food, Vol.3, No.1, pp. 20-24, 2010.

[3] H. Yaguchi, K. Nagahama, T. Hasegawa, and M. Inaba, "Development of An Autonomous Tomato Harvesting Robot with Rotational Plucking Gripper," 2016 IEEE/RSJ Int. Conf. on Intelligent Robots and Systems, pp. 652-657, 2016.

[4] T. Yoshida, T. Fukao, and T. Hasegawa, "Fast Detection of Tomato Peduncle Using Point Cloud with a Harvesting Robot," J. Robot. Mechatron., Vol.30, No.2, pp. 180-186, 2018.

[5] T. Fukatsu and M. Hirafuji, "Field Monitoring Using Sensor-Nodes with a Web Server," J. Robot. Mechatron., Vol.17, No.2, pp. 164-172, 2005.

[6] R. Fukui, K. Kawae, and S. Warisawa, "Development of a Tomato Volume Estimating Robot that Autonomously Searches an Appropriate Measurement Position – Basic Feasibility Study Using a

Tomato Bed Mock-Up –," J. Robot. Mechatron., Vol.30, No.2, pp. 173-179, 2018.

[7] K. Choi, G. Lee, Y. J. Han, and J. M. Bunn, "Tomato Maturity Evaluation Using Color Image Analysis," American Society of Agricultural Engineers, Vol.38, No.1, pp. 171-176, 1995.

[8] D. Kusui, H. Shimazu, K. Suezawa, and A. Shinjo, "A Novel Agricultural Skill Learning Support System and its Development and Evaluation," 2018 Joint 10th Int. Conf. on Soft Computing and Intelligent Systems and 19th Int. Symp. on Advanced Intelligent Systems, pp. 1020-1025, 2018.

[9] K. Wakamori and H. Mineno, "Optical Flow-Based Analysis of the Relationships between Leaf Wilting and Stem Diameter Variations in Tomato Plants," Plant Phenomics, Vol.2019, Artile ID 9136298, 2019.

[10] T. Fujinaga, S. Yasukawa, B. Li, and K. Ishii, "Image Mosaicing Using Multi-Modal Images for Generation of Tomato Growth State Map," J. Robot. Mechatron., Vol.30, No.2, pp. 187-197, 2018.

[11] T. Fujinaga, S. Yasukawa, and K. Ishii, "System Development of Tomato Harvesting Robot Based on Modular Design," 2019 Int. Workshop on Smart Info-Media Systems in Asia, SS1-1, pp. 1-6, 2019.

[12] R. F. Teimourlou, A. Arefi, and A. M. Motlagh, "A Machine Vision System for the Real-Time Harvesting of Ripe Tomato," J. of Agricultural Machinery Science, Vol.7, No.2, pp. 159-164, 2011.

[13] K. Hatou and Y. Hashimoto, "Recognition System for Tomato Fruits Based on the Wire Size Reduction Using Thermal Image," Environmental Control in Biology, Vol.40, No.1, pp. 75-80, 2002 (in Japanese).

[14] L. Wang, B. Zhao, J. Fan, X. Hu, S. Wei, Y. Li, Q. Zhou, and C. Wei, "Development of a tomato harvesting robot used in greenhouse," Int. J. of Agricultural and Biological Engineering, Vol.10, No.4, pp. 140-149, 2017.

[15] T. Fujiura, S. Nakao, N. Kondo, M. Dohi, and J. Yamashita, "Dichromatic 3-D Vision Sensor for the Agricultural Robot," J. of Japanese Society of Agricultural Technology Management, Vol.2, No.1, pp. 59-64, 1995 (in Japanese).

[16] K. Yamamoto, W. Guo, Y. Yoshioka, and S. Ninomiya, "On Plant Detection of Intact Tomato Fruits Using Image Analysis and Machine Learning Methods," Sensors, Vol.14, No.7, pp. 12191-12206, 2014.

[17] N. Kondo, "Selection of Suitable Wavelength Bands for Discrimination between Parts of Plant Body Using Their Spectral Reflectances," Environmental Control in Biology, Vol.26, No.4, pp. 175-183, 1988 (in Japanese).

[18] M. Monta, N. Kondo, S. Arima, and K. Namba, "Robotic Vision for Bioproduction Systems," J. Robot. Mechatron., Vol.15, No.3, pp. 341-348, 2003.

[19] B. Li, J. Lecourt, and G. Bishop, "Advances in Non-Destructive Early Assessment of Fruit Ripeness towards Defining Optimal Time of Harvest and Yield Prediction – A Review," Plants, Vol.7, No.3, 2018.

[20] T. Ota, S. Hayashi, K. Kubota, K. Ajiki, T. Komeda, and S. Otsuka, "Tomato Fruit Detection System Using Specular Reflection," J. of the Japanese Society of Agricultural Machinery, Vol.67, No.6, pp. 95-104, 2005 (in Japanese).

[21] N. Dalal and B. Triggs, "Histograms of Oriented Gradients for Human Detection," 2005 IEEE Computer Society Conf. on Computer Vision and Pattern Recognition, pp. 886-893, 2005.

[22] C. Cortes and V. Vapnik, "Support-Vector Networks," Machine Learning, Vol.20, pp. 273-297, 1995.

[23] Y. LeCun, L. Bottou, Y. Bengio, and P. Haffner, "Gradient-Based Learning Applied to Document Recognition," Proc. of the IEEE, Vol.86, No.11, pp. 2278-2324, 1998.

[24] C. Szegedy, W. Liu, Y. Jia, P. Sermanet, S. Reed, D. Anguelov, D. Erhan, V. Vanhoucke, and A. Rabinovich, "Going deeper with convolutions," 2015 IEEE Conf. on Computer Vision and Pattern Recognition, 2015.

[25] D. Comaniciu and P. Meer, "Mean Shift: A Robust Approach Toward Feature Space Analysis," IEEE Trans. on Pattern Analysis and Machine Intelligence, Vol.24, No.5, pp. 603-619, 2002.

[26] S. Ren, K. He, R. Girshick, and J. Sun, "Faster R-CNN: Towards Real-Time Object Detection with Region Proposal Networks," Advances in Neural Information Processing Systems, pp. 91-99, 2015.

[27] W. Liu, D. Anguelov, D. Erhan, C. Szegedy, S. Reed, C.-Y. Fu, and A. C. Berg, "SSD: Single Shot MultiBox Detector," European Conf. on Computer Vision, pp. 21-37, 2016.

Supporting Online Materials:

[a] ImageNet. http://www.image-net.org [Accessed July 29, 2020]

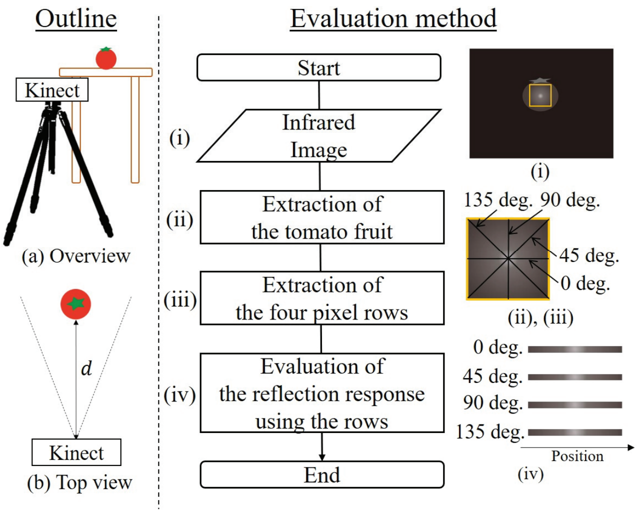

Fig. 14. Outline and evaluation method of the experiments to investigate the reflection response of tomato fruits.

Appendix A. Reflection Response of Tomato Fruits on Infrared Images

This appendix describes the experiments conducted to investigate the reflection response of tomato fruits to the infrared light projected by Kinect. In these experiments, we investigated the reflection response when the maturity stages were changed and the distance between the Kinect and tomato fruits was changed.

The outline and evaluation method for the experiments are shown in **Fig. 14**. The experiments were conducted one at a time with tomato fruits placed on a desk. The distance between the tomato fruits in the target cultivation area and the Kinect mounted on the robot was between 60 to 80 cm when the robot moved on rails in the tomato greenhouse. Therefore, for the distance d between the tomato fruits and the Kinect in **Fig. 14(b)**, three scenarios were considered: 60, 70, and 80 cm. For each distance, 30 tomato fruits were used: five tomato fruits each for six different maturity stages (Green, Breakers, Turning, Pink, Light Red, and Red).

To evaluate the reflection response, the 21×21 pixel region centered on the middle of the tomato fruit in the image, which was the position that responded most strongly to infrared light, was extracted from the infrared image (processes (i) and (ii), **Fig. 14**). Here, 21×21 pixel was the resolution of tomato fruits when d was 60–80 cm. With a horizontal line (0°) that passed through the center point of the extracted image and lines that were tilted by 45°, 90°, and 135° from the horizontal line, the pixel rows corresponding to the four lines were extracted (process (iii), **Fig. 14**). The extracted pixel rows were used to evaluate the response of tomato fruits to the infrared image (process (iv), **Fig. 14**). Here, the data type of the infrared image acquired by Kinect was uint (unsigned integer) 16, but for convenience, by normalizing from 0.0 to 1.0, this value was used as the response for each position of the pixel row.

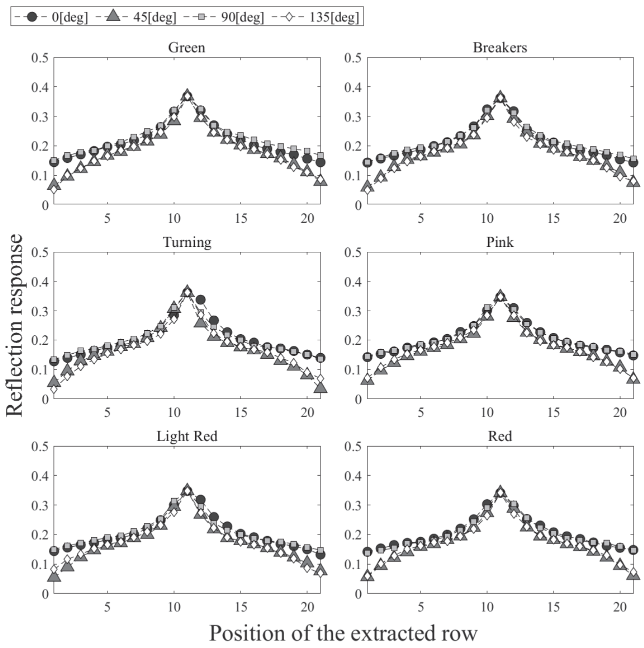

(a) Darkroom

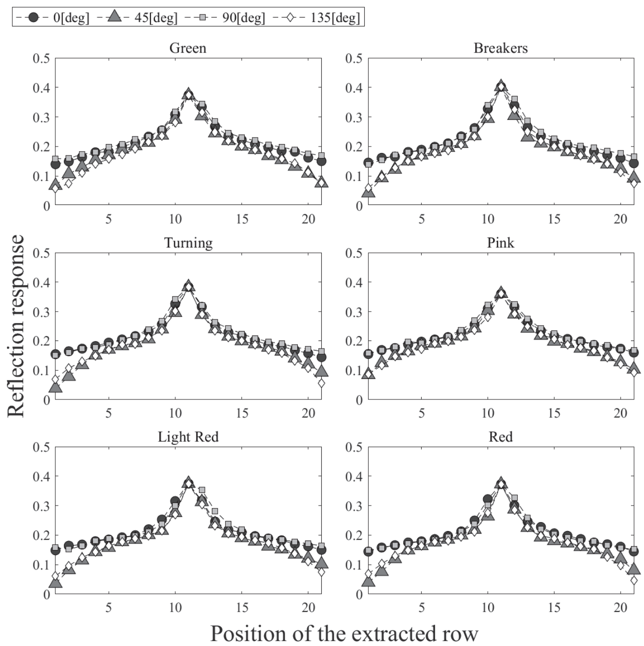

(b) Tomato greenhouse

Fig. 15. Response results of each pixel row for six different maturity stages at a d of 60 cm.

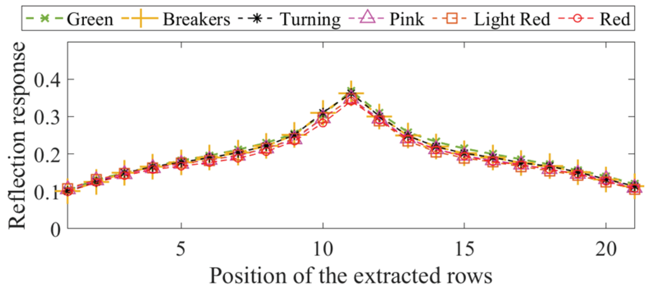

(a) $d = 60$ cm

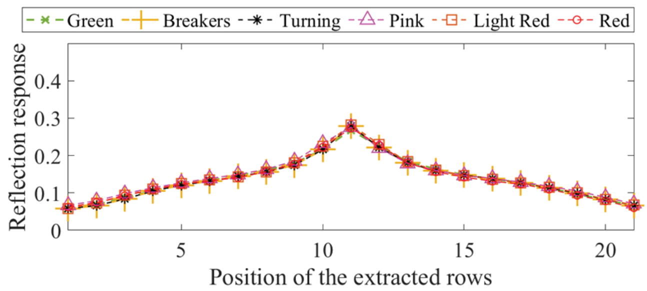

(b) $d = 70$ cm

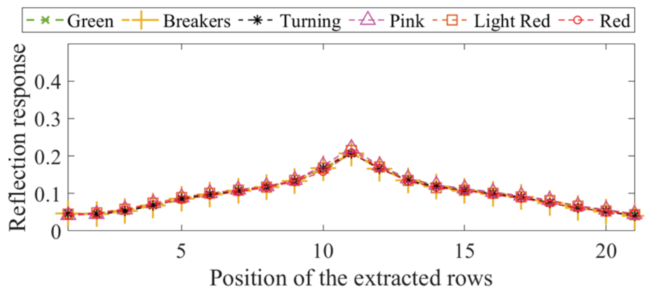

(c) $d = 80$ cm

Fig. 16. Response results for each maturity stage when the d changed in the darkroom.

Experiments were conducted in two places, i.e., in a darkroom and in a tomato greenhouse, to confirm the changes in the response owing to the difference in the effect of ambient light. The illuminance in the darkroom was 0.0 lx, and the illuminance in the tomato greenhouse was 8.2k lx. The illuminance in the tomato greenhouse was the average of 90 image acquisitions (six (maturity stages) $\times$ five (number of tomato fruits) $\times$ three (d)), and the standard deviation of 0.7k lx.

Figure 15 shows the response results of each pixel row for six different maturity stages at the d of 60 cm. The response results for each pixel row in **Fig. 15** were the average value for each position of five tomato fruits. **Figs. 15(a)** and **(b)** show the results for the darkroom and greenhouse, respectively. **Fig. 16** shows the response results of each maturity stage of the tomato fruits in the darkroom, and **Fig. 17** shows the results in the tomato greenhouse for a changing d. The response results at each maturity stage in **Figs. 16** and **17** are the average values at each position of all pixel rows for five tomato fruits.

The figures indicate that the response to infrared light exhibited the same tendencies regardless of the maturity stages of the tomato fruits in **Fig. 15**, i.e., the response at the center of the fruits was high and the surrounding area was weaker than the center of the fruits. In addition, under the conditions of these experiments, we confirmed that the same tendency in reflection response in both the darkroom and tomato greenhouse. **Figs. 16** and **17** indicate that the intensity of reflection response changed, but the transition of reflection response did not change even if the distance between tomato fruits and the Kinect changed.

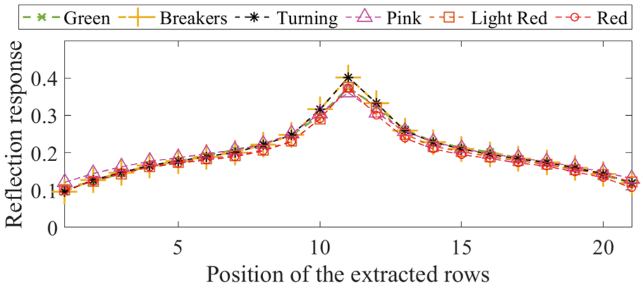

(a) $d = 60$ cm

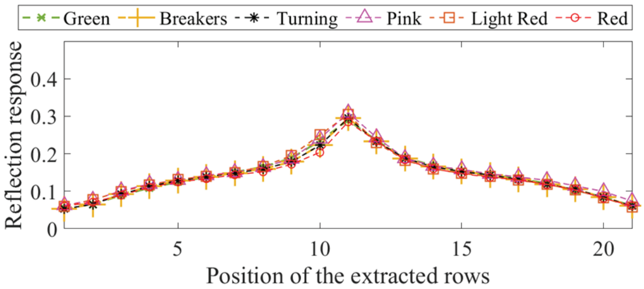

(b) $d = 70$ cm

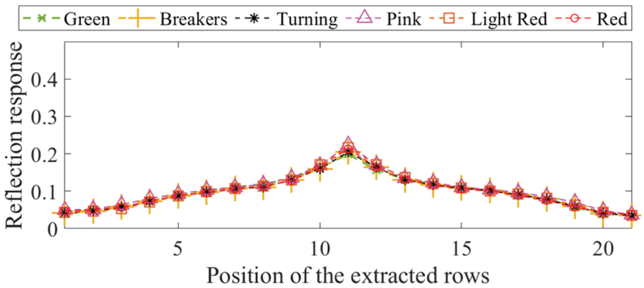

(c) $d = 80$ cm

Fig. 17. Response results for each maturity stage when the d changed in the tomato greenhouse.

Name:
Takuya Fujinaga

Affiliation:
Department of Life Science and Systems Engineering, Kyushu Institute of Technology

Address:
2-4 Hibikino, Wakamatsu, Kitakyushu, Fukuoka 808-0196, Japan

Brief Biographical History:
2016 Received Bachelor's degree from Department of Mechanical Information Science and Technology, Computer Science and Systems Engineering, Kyushu Institute of Technology
2018 Received Master's degree from Department of Human Intelligence Systems, Graduate School of Life Science and Systems Engineering, Kyushu Institute of Technology
2018- Doctoral Candidate in Department of Life Science and Systems Engineering, Graduate School of Life Science and Systems Engineering, Kyushu Institute of Technology

Main Works:
• "Image Mosaicing Using Multi-Modal Images for Generation of Tomato Growth State Map," J. Robot. Mechatron., Vol.30, No.2, pp. 187-197, 2018.

Membership in Academic Societies:
• The Japan Society of Mechanical Engineers (JSME)

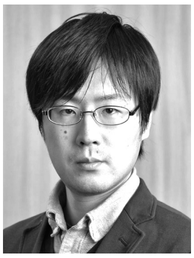

Name:
Shinsuke Yasukawa

Affiliation:
Associate Professor, Department of Human Intelligence Systems, Kyushu Institute of Technology

Address:
2-4 Hibikino, Wakamatsu, Kitakyushu, Fukuoka 808-0196, Japan

Brief Biographical History:
2014-2017 Research Associate, Kyushu Institute of Technology
2017 Received Ph.D. from Division of Electrical, Electronic and Information Engineering, Osaka University
2017-2018 Research Associate, The University of Tokyo
2018- Associate Professor, Kyushu Institute of Technology

Main Works:
• "Real-Time Object Tracking Based on Scale-Invariant Features Employing Bio-Inspired Hardware," Neural Networks, Vol.81, pp. 29-38, 2016.
• "Vision system for an autonomous underwater vehicle with a benthos sampling function," J. Robot. Mechatron., Vol.30, No.2, pp. 248-256, 2018.

Membership in Academic Societies:
• The Institute of Electrical and Electronics Engineers (IEEE)
• The Robotics Society of Japan (RSJ)

Name:
Kazuo Ishii

Affiliation:
Professor, Department of Human Intelligence Systems, Kyushu Institute of Technology

Address:
2-4 Hibikino, Wakamatsu, Kitakyushu, Fukuoka 808-0196, Japan

Brief Biographical History:
1996- Researcher, Institute of Industrial Science, The University of Tokyo
1996-1998 Assistant Professor, Kyushu Institute of Technology
1998-2011 Associate Professor, Kyushu Institute of Technology
2011- Professor, Kyushu Institute of Technology

Main Works:
• "An Optical Image Transmission System for Deep Sea Creature Sampling Missions Using Autonomous Underwater Vehicle," IEEE J. of Oceanic Engineering, Vol.45, Issue 2, pp. 350-361, 2020.
• "Image Mosaicing Using Multi-Modal Images for Generation of Tomato Growth State Map," J. Robot. Mechatron., Vol.30, No.2, pp. 187-197, 2018.

Membership in Academic Societies:
• The Institute of Electrical and Electronics Engineers (IEEE)
• The Japan Society of Mechanical Engineers (JSME)
• The Robotics Society of Japan (RSJ)
• The Japan Society of Naval Architects and Ocean Engineers (JSNAOE)